Oehlschlägel *et al.*
Microplastics and Nanoplastics (2024) 4:1
https://doi.org/10.1186/s43591-023-00079-x

Microplastics and Nanoplastics

RESEARCH

Open Access

Water–air transfer rates of microplastic particles through bubble bursting as a function of particle size

Lisa Marie Oehlschlägel[1], Sebastian Schmid[1], Moritz Lehmann[2], Stephan Gekle[2] and Andreas Held[1*]

Abstract

Microplastic (MP) particles can be ejected into the air by jet drops when gas bubbles burst at water surfaces. For a qualitative and quantitative understanding of this transport mechanism from the hydrosphere to the atmosphere, we studied the transfer of MP due to bubble bursting at the air–water interface in laboratory experiments. Gas bubbles were produced with filtered air that was pushed through a stainless-steel frit at two different volume flow rates in a glass flask filled with polystyrene (PS) particles of six different diameters (0.35 µm, 0.5 µm, 0.75 µm, 1 µm, 1.5 µm, 2 µm) suspended in deionized water. Airborne PS particle concentrations were measured by an optical particle counter. Additionally, size and volume of the bursting bubbles and the resulting jet droplets were analyzed with a camera. Depending on the volume flow rates, bubble bursting rates from 688 s^{-1} to 1176 s^{-1} and mean diameters of the bursting bubbles from 0.76 mm to 0.81 mm were observed. The mean diameters of the top jet drops were estimated to be between 0.10 mm and 0.11 mm. The measured number of jet droplets ranged from 2092 s^{-1} to 2391 s^{-1}. For particle diameters from 0.35 µm – 2.0 µm, the airborne MP particle concentrations ranged from 4.2 l^{-1} to 348 l^{-1}. We determined size-dependent transfer factors for the water–air transfer and found a maximum for 1 µm particles. For MP particles up to 1 µm diameter, the particle concentration in the jet droplets was enhanced compared to the bulk water concentration, indicating an enrichment of MP particles at the water–air-interface of bubbles.

Keywords Airborne microplastic, Atmospheric microplastic, Jet drops, Particle ejection, Laboratory experiments

Introduction

Approximately 10^{18} – 10^{20} bubbles burst every second over the oceans [22]. Whitecaps and breaking waves are the main sources of gas bubbles in the oceans, with bubble sizes ranging from smaller than 0.1 mm to approximately 10 mm [10]. Bubble bursting generates sea spray aerosols (e.g. [17]), and inorganic salts, organic matter as well as bacteria and viruses are efficiently transferred from the water into the air by this mechanism (e.g. [3, 8, 31]). Since microplastic (MP) particles are abundant in ocean water (e.g. [13]), on shorelines [12] and in ocean sediment [41], it can be expected that bubble bursting is an efficient process for MP transfer from oceans to the atmosphere (e.g. [2, 26, 38]). Currently, this process is poorly quantified and recent studies such as Masry et al. [27] point out that MP transfer rates must be quantified in order to evaluate the relevance of bubble bursting as a source for atmospheric MP. Atmospheric MP particles are considered a potential risk to human health [14, 30], and may also be a vector for toxic substances added or attached to MPs [16, 20].

At the water surface, bubbles burst and film droplets develop from the surface water film when the bubble exceeds a diameter of approximately 2.4 mm [37]. For bubbles with diameters less than 3 mm, the film simply

*Correspondence:
Andreas Held
held@tu-berlin.de
[1] Environmental Chemistry and Air Research, Technische Universität Berlin, Environmental Chemistry and Air Research, KF3, Straße des 17. Juni 135, Berlin 10623, Germany
[2] Biofluid Simulation and Modeling, University of Bayreuth, Bayreuth, Germany

rolls up [36]. In addition, one or multiple jet drops are formed due to the collapse of the bubble cavity [37]. The top jet drop is the largest and fastest drop [22, 35], and may be ejected up to a height of 20 cm for a ~ 2 mm bubble in salt water [10].

It has been postulated that the composition of film drops is influenced by the sea surface microlayer, while jet drops represent the bulk water composition (e.g. [39]). The sea surface microlayer is known to be enriched in hydrophobic compounds such as organic matter (e.g. [18, 40]), and also MP particles (e. g. [4, 13, 34]). Anderson et al. [4] report an enrichment of approximately an order of magnitude of MP particles in the sea surface microlayer of two estuaries compared to bulk water. Chae et al. [13] observed higher MP particle concentrations in the sea surface microlayer compared to bulk surface water off the Western Korean coast, and Song et al. [34] found a strongly enhanced MP concentration in the sea surface microlayer compared to conventional Manta trawl sampling off the Southern Korean coast.

Particles transported from the ocean into the air via bubble bursting (e.g. [33]) can be picked up by wind and transported to more distant areas [2]. Various studies have detected atmospheric MP particles in remote areas (e.g. [1, 11]), and in recent years, further studies have identified MP in the marine boundary layer [2, 19, 23, 26, 38, 42]. Liu et al. [26] sampled suspended atmospheric MP during a cruise in the west Pacific Ocean and detected 0 to 1.37 particles per cubic meter of air. Allen et al. [2] sampled air in the marine boundary layer on the Atlantic coast in France. The average concentration of MP particles found in onshore winds was 2.9 m^{-3}, and in offshore winds 9.6 m^{-3}. Trainic et al. [38] sampled aerosols in the North Atlantic Ocean and found atmospheric MP particles with estimated atmospheric residence times from 5 min to 2 days in 20% of their samples.

In laboratory experiments, Quinn et al. [31] studied the water–air transfer of 0.48 µm and 0.79 µm polystyrene particles in jet drops produced by bubble bursting. In their experiments, they found that the particle concentration in the jet drop was basically independent of the particle concentrations in the bulk water but increased with the bubble age. Similarly, Sakai et al. [32] found an enrichment of 0.5 µm latex particles in the surface layer of rising bubbles, and in jet drops. Recently, Masry et al. [27] showed that 0.35 µm polystyrene particles are transferred from water to air by bubble bursting. They also used 0.6 µm and 1 µm particles but could not clearly confirm water–air transfer of these larger particles, and they conclude that MP particle transfer rates could bring answers to the significance of bubble bursting as a source of atmospheric MP particles.

We hypothesize that bubble bursting is an efficient water–air transfer process of MP particles. The goal of this study is to quantify the water–air transfer of MP particles as a function of particle size by the bubble bursting process. To this end, we present results of laboratory experiments with well-defined bubble populations and pre-defined concentrations of polystyrene (PS) particles with diameters between 0.35 µm and 2 µm suspended in water. Specifically, we quantify size-dependent transfer rates of MP particles, and analyze bubble and jet drop size distributions in order to contribute to estimating an order of magnitude of the global emission of atmospheric MP particles from oceans by bubble bursting.

Methods

General setup of bubble bursting experiments

We set up experiments to generate small gas bubbles in water with varying concentrations of MP particles, and to measure the number concentration of particles transferred from the water into the air due to the bubble bursting process (Fig. 1).

A glass flask with a total volume of 2.45 l was filled with 1 l of deionized water (Seradest S750, conductivity $\kappa < 0.1$ µS cm^{-1}) at room temperature, resulting in a total water column of 8 cm. Deionized water was used to reduce the production of polydisperse airborne salt particles from drying droplets. The water volume was mixed with 0.1 to 5 ml of aqueous suspensions of monodisperse spherical polystyrene (PS) particles (Polybead Microspheres, Polysciences, Hirschberg an der Bergstraße, Germany) containing 2.5% solids and a small amount of proprietary surfactant. Six different particle diameters in the diameter range from 0.35 µm to 2 µm (0.35 µm, 0.5 µm, 0.75 µm, 1 µm, 1.5 µm, 2 µm) were used. The particles contain a slight anionic surface charge from sulfate ester groups [29]. The MP particle suspensions were filled into small glass vials, and defined volumes were taken with a microliter pipette in order to produce a bulk concentration of approximately 10^{11} particles per liter of water for particle diameters from 0.35 µm to 1 µm. For 1.5 µm and 2 µm particles, the bulk concentration was approximately 3×10^{10} l^{-1}, and for 0.5 µm, an additional experiment with an increased particle concentration of approximately 3×10^{11} l^{-1} was prepared (details in Table S1, Supplementary material). The pipette volume was discharged into the glass flask, and the water was stirred for uniform particle distribution. The MP particle density of 1.05 g cm^{-3} is slightly larger than the density of water.

Before and after each experimental run, the glass flasks and all materials that came in contact with the water and the suspended MP particles were cleaned by thoroughly rinsing with deionized water and detergent, and again with deionized water. At the beginning

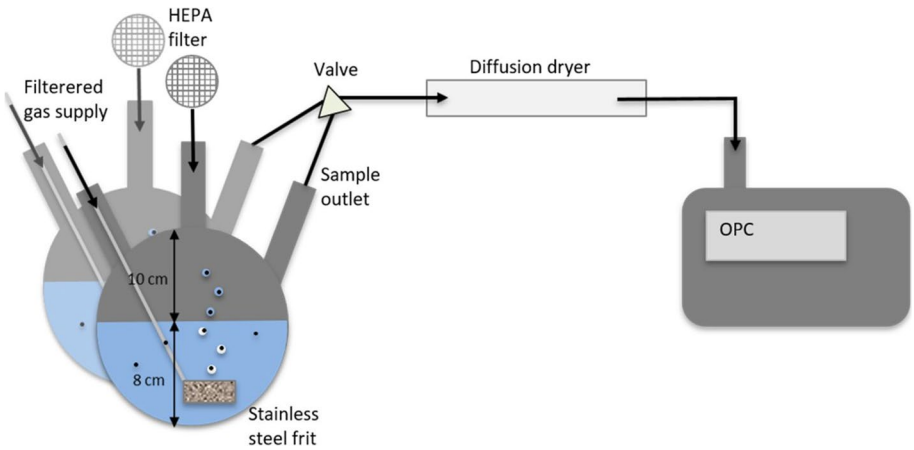

Fig. 1 Schematic representation of the experimental setup including two glass flasks with filtered gas supply and a stainless-steel frit to produce bubbles (white) in water with MP particles (black), and droplets (blue) in the headspace. Sample air is transferred through a diffusion dryer to an optical particle counter (OPC). The valve is switching between the two flasks every 15 min

of the experiment, the headspace with a volume of 1.45 l was free of particles. In order to produce gas bubbles, filtered (NY Simplepure syringe filter; 0.45 µm, Membrane Solutions LLC., USA) room air was pushed through a stainless-steel frit (IDEX Health & Science, Oak Harbor, WA, USA) with a pore size of 20 µm with a peristaltic pump (IPS-8, Ismatec SA, Glattbrugg-Zürich, Switzerland) at two different pumping rates. The volume flow rates (VFR) corresponding to the two pumping rates measured with a bubble flowmeter (mini-Buck-Calibrator M-5, A.P. Buck Inc., Orlando, Florida, USA) were 182 $mm^3\ s^{-1}$ [50 RPM] and 353 $mm^3\ s^{-1}$ [90 RPM]. Depending on the pumping rate, this produced a population of small air bubbles bursting in an area of approximately 50 cm^2. Thus, the air flux rate per unit area of water surface was 36.4 and 70.6 ml $m^{-2}\ s^{-1}$, respectively. The mean bubble diameter ranged from 0.76 mm to 0.81 mm with maximum diameters up to 2.72 mm, thus producing mostly jet drops after bubble bursting. With a volume flow rate of 1.2 l min^{-1}, air was sampled from the headspace of the glass flask through a dryer to an optical particle counter. Droplets were dried with a Nafion diffusion dryer (Perma Pure MD-110-24S-4, Lakewood, NJ, USA) and introduced into an optical particle counter (OPC, Mini Laser Aerosol Spectrometer 11-R, Grimm Aerosoltechnik, Ainring, Germany) to measure the particle number size distribution in 31 size channels between 0.25 and 32 µm particle diameter with a sampling interval of 6 s. A HEPA filter was added to the glass flask to compensate for the difference of the OPC sample flow rate and the volume flow rate for generating gas bubbles. Note that the volume flow rate from the glass flask to the OPC is much higher than the volume flow rate used to generate bubbles, and thus, air flow through the HEPA filter is always directed into the glass flask. No particles or droplets are lost to the HEPA filter. In each experimental run, two experiments with different MP particle diameters were run in parallel. Two glass flasks were filled with deionized water taken out of a glass tank that was bottled before all experiments to guarantee the same water quality for all experiments. Suspensions of MP particles with different diameters were added to each flask according to Table S1 (Supplementary material). Both glass flasks were connected to the diffusion dryer and the OPC through a pinch valve that switched the sample flow between the two flasks every 15 min. In order to remove all particles from the headspace in the flasks, the OPC sampled air alternating every 15 min between the two glass flasks until the average total particle concentration was less than 1 l^{-1}. Then, the peristaltic pump was turned on for one hour with a VFR of 353 $mm^3\ s^{-1}$ before data was collected for evaluation. After the one-hour lead time, the experiments were carried out for 300 min with VFR 182 $mm^3\ s^{-1}$ and 353 $mm^3\ s^{-1}$, respectively. In total, this resulted in 10×15 min sample intervals per glass flask and VFR. For each particle diameter, two experiments with different particle concentrations in water were carried out. Depending on the experiment, an increased background particle concentration was measured in the diameter range from 0.25 µm to 0.5 µm. In order to take into account this particle background, the particle concentration measured in parallel in the diameter range of interest in the flask without MP particles of this diameter was considered as a background concentration from the particle concentration.

Characterization of air bubbles and jet droplets

To analyze the number of rising bubbles, the size of bursting bubbles and of the resulting jet droplets, a standard camera (Panasonic DC-FZ82) with a resolution of 1280 pixel × 720 pixel and a frame rate of 100 frames per second was used in three different arrangements with illumination by high-power LEDs as shown schematically in Fig. 2.

In order to count the number of rising bubbles, the camera was directed at the setup from the side, and the setup was illuminated from the back (Fig. 2a, d). Overlapping bubbles were identified and marked separately from individual bubbles. Recording of the water surface from the top allowed capturing the bursting bubbles (Fig. 2b, e). To block interference with lower ascending bubbles in the tank, the illumination was restricted to a thin layer on the surface by using LEDs in combination with slit blinds. Size was calibrated by using a benchmark at the surface level. The resulting video material was then analyzed using computer vision to detect and track individual bubbles. Thresholding the image based on brightness values resulted in isolated bubble contours. However, those contours can either belong to single bubbles or clustered bubbles and require segmentation. The segmentation was done following an algorithm proposed by Bettaieb et al. [6]. In contrast to the proposed algorithm, start and end points of individual segments were identified by convexity defects of the bubble shapes. As individual segments can belong to the same bubble, they were matched and recombined. This involved fitting circles to each segment. The fitted circles were then compared to every other segment in the corresponding cluster. Identical geometry and center coordinates (within a tolerance of ± 25% of bubble radius) indicated contour segments belonging to a single bubble. Estimated center coordinates and radii were matched between previous and current frames to track bubble movement. Matching was done by using a simple linear movement estimation from the last two frames of a bubble. The estimated position was then matched with the currently detected bubbles by shortest distance but limited by the maximum distance a bubble could reasonably travel within a frame to avoid wrong matching. Using this method allowed following individual bubbles until no more match was detected, indicating that the bubble of interest burst or merged. To check whether the lost bubble did in fact burst and not merge into a bubble nearby, all surrounding bubbles were checked for an increase in size. If so, the lost bubble was marked as merged and did not contribute to further analysis. According to Kočárková et al. [24], the shape of small bubbles can be approximated by a sphere for Bond numbers up to 0.25, which corresponds to bubble diameters up to approximately 2.7 mm for air bubbles in water at room temperature. Image resolution in the rising bubble setup (Fig. 2a) led to a pixel-length conversion factor of 19 µm/pixel.

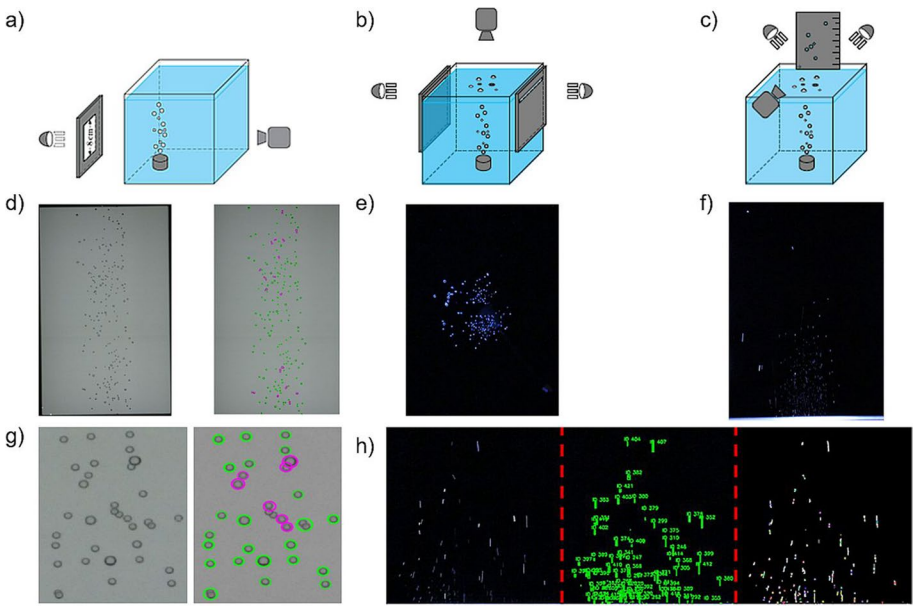

Fig. 2 Schematic setup (**a**) to quantify the number of rising bubbles (camera from side and back illumination), (**b**) to quantify the bursting bubble diameters (camera from top and illumination from side), and (**c**) to capture the trajectories of resulting jet droplets (camera from front and illumination from side). Raw images of (**d**) rising bubbles (individual bubbles in green, overlapping bubbles in magenta), (**e**) bursting bubbles, (**f**) jet droplets; (**g**) enlarged view of raw image of rising bubbles and captured bubble shapes (individual bubbles in green, segmented bubbles in magenta); (**h**) raw video image of jet droplets (left), tracked droplets (center) and processed droplet position (right)

For the characterization of jet droplets, the camera was directed at the setup from the front, and illumination with high-power LEDs from the side (Fig. 2c, f). Overlapping and merging of droplets was neglected. However, the droplet movement did produce motion blur in the image material. To estimate the droplet size, a rotated rectangle was fitted around the blurred droplets. Estimating that the deformation only occurred in the direction of movement, the shorter side of the rotated rectangle indicated the actual size of the droplet. Matching between previous and current frames was carried out as described above for bursting bubbles.

The image recognition of bursting bubbles and jet droplets in this study was technically limited. First, the detection of larger bubbles was limited under poor lighting conditions, which may have led to bubbles with diameters over 1 mm being detected as several smaller bubbles. This was caused by irregular illumination from point light sources on the edges of the rectangular basin. Second, the resolution of the video material was not sufficient to accurately detect and quantify the sizes of bubbles and droplets with diameters below 0.4 mm. In the bursting bubble setup (Fig. 2b), the pixel-length conversion factor was 104 µm/pixel, and in the droplet setup (Fig. 2c), the conversion factor was 172 µm/pixel. The minimum resolved bubble diameter was 0.32 mm, and the minimum resolved droplet diameter was 0.15 mm. In general, the number of bubbles and droplets in the smallest size classes may be underestimated.

Data analysis and calculations

Airborne MP particle concentrations were calculated from the observed OPC particle size distributions. For each of the six particle diameters used in this study, the corresponding size channels of the OPC were evaluated individually. In each 15 min sampling interval, the first 5 min after switching the valve were discarded. The remaining data were averaged separately for each experiment and each VFR.

The expected airborne MP concentration were calculated assuming that particle input into the flask headspace is only from drying droplets generated by bubble bursting, and particles are removed from the flask headspace only with the sampling flow of the OPC. In this evaluation, there is no differentiation between film drops, the top jet drop and following secondary jet drops.

The input of airborne particles into the flask headspace, dN_{in}/dt [s^{-1}], is estimated by Eq. 1,

$$\frac{dN_{in}}{dt} = \frac{N_w}{V_w} \bullet Q_d \bullet f_{w-a} \tag{1}$$

with N_w, number of MP particles in the water volume V_w [mm^3], Q_d, rate of droplet volume generated per second [$mm^3\ s^{-1}$], and $f_{w\text{-}a}$ a dimensionless transfer factor that takes into account the effective water – air transfer of MP particles.

The number of particles removed from the flask headspace per unit time, dN_{out}/dt, is estimated by Eq. 2,

$$\frac{dN_{out}}{dt} = \frac{N_a}{V_a} \bullet Q_a \tag{2}$$

with N_a, number of MP particles in the headspace volume V_a [mm^3], Q_a, air sampling flow rate [$mm^3\ s^{-1}$].

For steady state conditions, the steady-state concentration of particles in the headspace can be calculated by equating the particle input and output fluxes of Eqs. 1 and 2, and solving for N_a/V_a:

$$\frac{N_a}{V_a} = \frac{N_w}{V_w} \bullet \frac{Q_d}{Q_a} \bullet f_{w-a} \tag{3}$$

In this study, the water volume is $V_w = 10^6$ mm^3 (= 1 l), the headspace volume is $V_a = 1.45 \times 10^6$ mm^3 (= 1.45 l), the sampling flow rate of the OPC is $Q_a = 2 \times 10^4$ $mm^3\ s^{-1}$ (= 1.2 l min^{-1}), the number of MP particles in the water volume N_w is taken from Table S1 (Supplementary material), and the droplet volume generated per second, Q_d, is estimated from the observed bubble and droplet size distributions (Bursting bubbles and jet droplets - number concentrations and size distributions). Note that the transfer factor $f_{w\text{-}a}$ is unknown; it is determined by equating observed and expected airborne MP concentration acc. Equation 3, N_a/V_a, and solving for $f_{w\text{-}a}$,

$$f_{w-a} = \frac{N_a}{V_a} \bullet \frac{V_w}{N_w} \bullet \frac{Q_a}{Q_d} \tag{4}$$

When switching the sampling flow between two glass flasks in 15 min intervals, the change in airborne MP particle number in one particular glass flask will be $N_{in} - N_{out}$ for the 15 min intervals when the sampling flow is taken from this glass flask, and N_{in} for the 15 min intervals when the sampling flow is taken from the other glass flask.

In addition to experimentally derived droplet size distributions, droplet size distributions were estimated from observed size distributions of bursting bubbles, by applying the universal scaling law for the top jet drop diameter, D_{jet}, as a function of the bursting bubble diameter, D_{bub}, as given by Gañán-Calvo [21]. These estimated droplet size distributions were used to calculate the droplet volume flux for fully evaporating droplets (more details in Size-dependent MP particle transfer rates). The ambient droplet volume flux of ocean sea spray has been calculated using the parameterization by Andreas [5] following environmental

Table 1 Overview of experimentally determined bubble burst rates, minimum, mean and maximum bubble diameters, volume of bursting bubbles and droplet production rates, mean and maximum droplet diameters, average number of droplets per bursting bubble, and volume of droplets generated per second for low and high VFR

	Low	High
VFR *[mm^3 s^{-1}]*	182	353
Air flux [ml/m^2/s^{-1}]	36.4	70.6
Burst rate [s^{-1}]	688	1176
$D_{bub,\ min}$ [mm]	0.48	0.32
$D_{bub,\ mean}$ [mm]	0.81	0.76
$D_{bub,\ max}$ [mm]	2.40	2.56
Burst volume rate [mm^3 s^{-1}]	265	362
Droplet rate [s^{-1}]	2092	2391
$D_{drop,\ mean}$ [mm]	0.42	0.48
$D_{drop,\ max}$ [mm]	2.46	4.15
Droplet volume rate Q_d [mm^3 s^{-1}]	159	340
Droplets per bubble [-]	3.0	2.0

observations by Monahan et al. [28]. Details of the calculation method can be found in the Supplementary material (S2).

Results and discussion

Bursting bubbles and jet droplets—number concentrations and size distributions

Under two different conditions to generate bubbles, the number of bursting bubbles increased with increasing volume flow rates from 688 bursts per second at the low VFR (182 mm^3 s^{-1}) to 1176 s^{-1} at the high VFR (353 mm^3 s^{-1}) (Table 1). Thus, the rate of bursting bubbles at the low VFR was about 59% of the high VFR.

While the number of bursting bubbles changed, the bubble size distributions were similar for the different VFRs. The mean diameter of the bursting bubbles ranged from 0.76 mm to 0.81 mm, with minimum diameters from 0.32 mm to 0.48 mm and maximum diameters from 2.40 mm to 2.72 mm (Table 1). The fraction of bubbles with diameters larger than 2.4 mm was negligible, and therefore mostly jet drop production is expected in these experimental conditions. Overall, the modal diameter

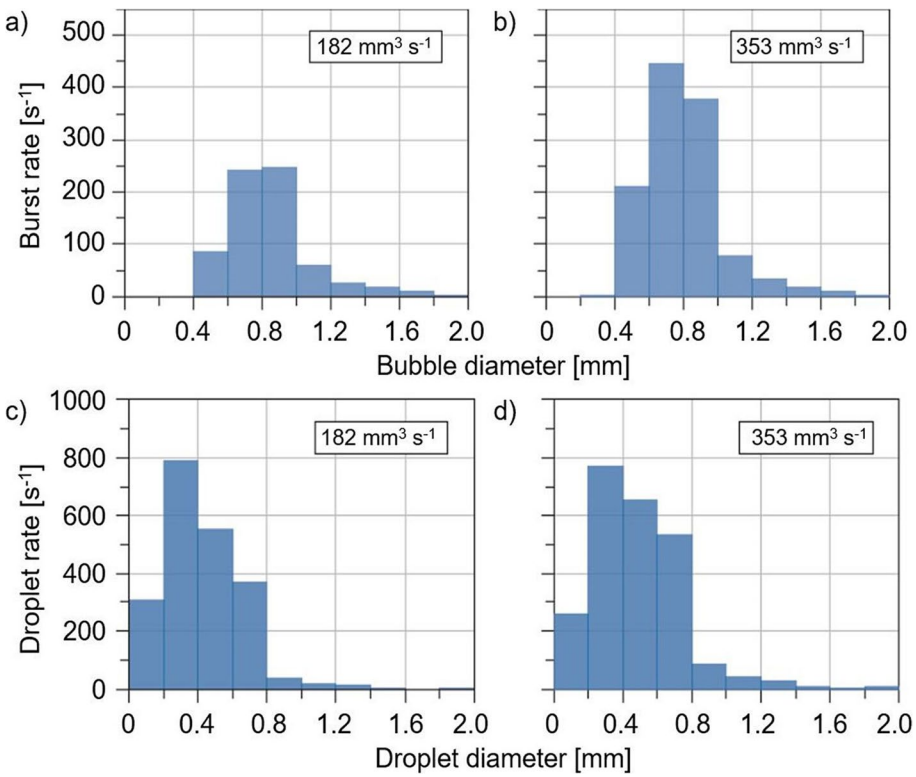

Fig. 3 Experimentally derived average size distributions of bursting bubbles at (**a**) VFR 182 mm^3 s^{-1} and (**b**) VFR 353 mm^3 s^{-1}, and average droplet size distributions at (**c**) VFR 182 mm^3 s^{-1} and (**d**) VFR 353 mm^3 s^{-1}. Note that the minimum resolved bubble diameter was 0.32 mm and the minimum resolved droplet diameter was 0.15 mm due to experimental limitations

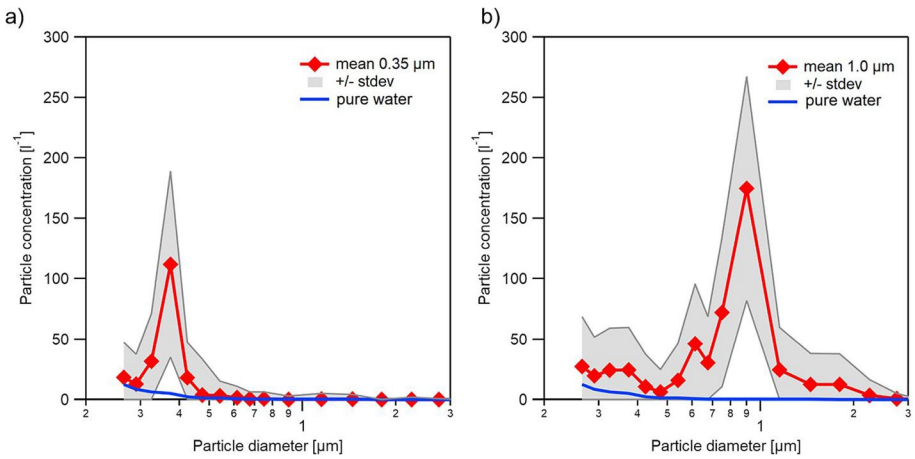

Fig. 4 Particle size distribution for experiments with (**a**) 0.35 µm diameter MP particles and (**b**) 1.0 µm diameter MP particles, VFR = 353 mm^3 s^{-1}. Blue line indicates size distribution of pure water

of the bursting bubbles was 0.6 mm. Figure 3a, b shows average bubble size distributions derived experimentally at two different VFRs.

In stationary behavior, the total volume of the observed bursting bubbles should correspond to the VFRs. As shown in Table 1, estimated burst volumes per second exceeded corresponding VFRs, indicating an overestimation of bubble number or size, especially with the lower VFR. Uncertainties might be introduced by the limited image resolution, which did not allow for precise segmentation of coalesced bubbles. Additionally, non-optimal lighting could lead to large bubbles being detected as several small bubbles. At higher VFR, the burst volume is only slightly overestimated, possibly due to the smaller relative influence of larger bubbles and coalescence with higher bubble counts. With varying burst rates of bubbles and similar bubble size distributions, an increasing droplet number and similar droplet diameters generated by bubble bursting for the two different VFRs is expected. Table 1 shows the experimentally determined number of droplets generated per second, the mean and maximum droplet diameter, the average number of droplets generated per bubble and the droplet volume rate for low and high VFRs. The droplet rate, i. e. the number of droplets generated per second, increases from 2092 s^{-1} to 2391 s^{-1}. Comparing with the burst rate, this yields on average 3.0 droplets per bursting bubble at VFR 182 mm^3 s^{-1} and 2.0 droplets per bubble at VFR 353 mm^3 s^{-1} (Table 1). Figure 3c, d shows average droplet size distributions for the two different VFRs. There is a slight increase in mean droplet diameter for the higher VFR from 0.42 mm to 0.48 mm, and the maximum droplet diameter increases from 2.46 mm to 4.15 mm. Consistent with the shift of the droplet size distribution to larger diameters, the mean volume of droplets generated per second increases from 159 mm^3 s^{-1} at low VFR to 340 mm^3 s^{-1} at high VFR.

The minimum droplet diameter that could be resolved with the experimental setup was 0.15 mm, and it was observed in both VFR setups. Taking into account Eqs. S2.1 and S2.2, the top jet droplet diameter can be expected to be smaller than 0.15 mm for bubble diameters smaller than 0.55 mm. Figure 3a, b indicates that a considerable fraction of the bubble size distributions was smaller than 0.55 mm. The bubble size distributions can be used together with Eqs. S2.1 and S2.2 to calculate an independent estimate for the diameters of the top jet droplets resulting from the bursting bubbles. This calculation yields a mean diameter of the top jet droplet of 0.11 mm for VFR 182 mm^3 s^{-1}, and 0.10 mm for 353 mm^3 s^{-1}, respectively.

Airborne MP concentrations

In order to identify water–air transfer of MP particles due to bubble bursting, size distributions of airborne particles in the head space of the glass flask were measured and analyzed for concentration increases in the size range of interest. For example, Fig. 4 shows average particle size distributions of two experiments with 0.35 µm and 1.0 µm MP particles. Significantly enhanced number concentrations can be seen in the diameter ranges around 0.35 µm and 1 µm, respectively. An example of the temporal evolution of the particle concentrations in the size channels corresponding to 0.35 µm and 1.0 µm diameter MP particles as well as the expected airborne MP concentration acc. Equations 1 – 3 can be found in Figure S3 (Supplementary material).

Enhanced particle concentrations in the corresponding size ranges were detected in all experiments. Figure 5

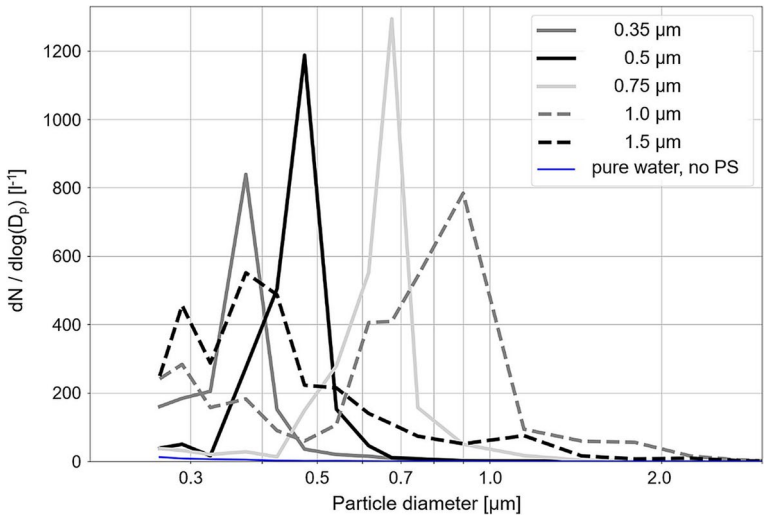

Fig. 5 Particle size distributions with MP particle diameters from 0.35 µm to 1.5 µm (black and grey) and pure water particle concentration (blue), VFR = 353 mm^3 $s.^{-1}$

Table 2 Observed MP particle concentrations in air for six different particle diameters D_p at VFR = 182 mm^3 s^{-1} and VFR = 353 mm^3 s^{-1}. Results for 0.5 µm particle diameter are for experiment with total number of 1.09×10^{11} particles in water volume

Particle diameter [µm]	MP concentration [l^{-1}]		Transfer factor $f_{w\text{-}a}$	
	VFR 182 mm^3 s^{-1}	VFR 353 mm^3 s^{-1}	VFR 182 mm^3 s^{-1}	VFR 353 mm^3 s^{-1}
0.35	88.6	165.2	1.67	0.14
0.5	143.3	248.8	2.63	0.20
0.75	126.0	252.4	2.33	0.20
1	147.2	348.3	3.24	0.33
1.5	9.2	24.6	0.68	0.08
2	4.2	14.3	0.29	0.04

shows average size distributions for five experiments with MP particle diameters from 0.35 µm to 1.5 µm, and one experiment with pure water without addition of MP suspensions. Local maxima of the particle size distributions can be clearly seen for the 0.35 µm, 0.5 µm, 0.75 µm and 1.0 µm MP particles. For larger MP particles, the concentration is still enhanced in the corresponding diameter range, but cannot be clearly distinguished from background measurements without MP particles. The size distributions in Fig. 5 indicate that the bubble bursting process also produces particles in size ranges not corresponding with the added MP particle diameters. Particles smaller than the nominal MP diameter are expected to be produced from minuscule impurities of the water and the liquid MP suspensions in drying droplets, yielding polydisperse airborne salt particles. In addition, agglomerates of monodisperse MP particles may contribute to the particle fraction larger than the nominal MP diameter.

The left part of Table 2 shows observed airborne particle concentrations of experiments with six different particle diameters and two different VFRs. As expected, the observed particle concentrations are higher in the experiments with higher VFR, and thus, higher burst rates and droplet production rates. The observed particle concentrations of 1.5 µm and 2 µm particles are in the range of background concentrations and should be treated with caution. Low concentrations of airborne MP particles of 1.5 µm and 2 µm diameter are expected due to the low concentration of these MP particles in the water volume (cf. Table S1, supplementary material). For experiments with MP particle diameters of 1 µm and less, the number concentration in water is close to 10^{11} l^{-1}, and changes in airborne MP particle number concentration indicate size-dependent effects in the water–air transfer.

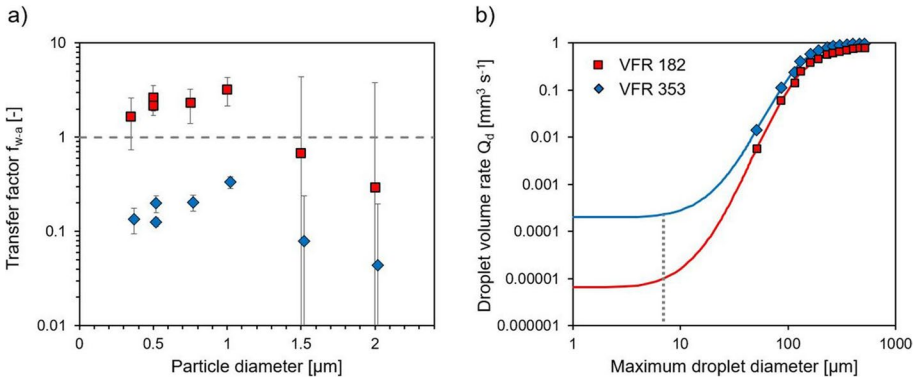

Fig. 6 **a**) Water–air transfer factors f_{w-a} as a function of particle diameter in the range from 0.35 µm to 2.0 µm, and **b**) droplet volume Q_d generated per second by all droplets with the given maximum droplet diameter. Results for low volume flow rates are shown in red, for high volume flow rates in blue. Error bars in 6a indicate uncertainty due to a variable background concentration of up to 50 particles per liter

Size-dependent MP particle transfer rates

Size-dependent water–air transfer factors of MP particles, f_{w-a}, are shown in Fig. 6a and in Table 2. Transfer factors f_{w-a} were calculated using Eq. 4, with the observed airborne MP concentrations given in Table 2, the water volume $V_w = 1$ l, the number of MP particles in the water volume N_w given in Table S1 (supplementary material), and the sampling flow rate of the OPC, $Q_a = 20$ ml s^{-1}.

The droplet volume generated per second, Q_d, can be estimated from the observed droplet size distributions (Fig. 3c, d) as given in Table 1, or from the droplet size distribution calculated based on the observed bubble size distributions using Eqs. S2.1 and S2.2. Most large droplets are expected to return to the water volume by gravitational settling before fully evaporating. Vertical air motion in the headspace of the glass flask is expected to be negligible, and the droplet settling time can be estimated by dividing the headspace height of 10 cm by the size-dependent gravitational settling velocity calculated acc. Eq. S2.3. For droplets larger than approximately 7 µm, the droplet settling time becomes smaller than the average residence time in the headspace, i.e. the headspace volume $V_a = 1.45$ l divided by the volume flow rate of the OPC, $Q_a = 20$ ml s^{-1}. Droplet diameters of 7 µm and below cannot be resolved in our droplet images due to the limited image resolution. Because of this limitation, we calculated the droplet size distribution based on the observed bubble size distribution, extrapolated the calculated droplet size distribution using a Weibull fit (Fig. 6b), and estimated the total volume of droplets smaller than 7 µm from this extrapolation, yielding $Q_{d,low} = 1.0 \times 10^{-5}$ mm^3 s^{-1} and $Q_{d,high} = 2.3 \times 10^{-4}$ mm^3 s^{-1} for the two different VFRs (indicated by the vertical broken line at 7 µm in Fig. 6b).

For each individual particle diameter, the experiments with the low VFR = 182 mm^3 s^{-1} (red squares in Fig. 6a) yield larger transfer factors than with the high VFR = 353 mm^3 s^{-1} (blue diamonds in Fig. 6a). While the bubble burst rate is 70% higher at high VFR compared to low VFR, the number of observed droplets is only 14% higher (cf. Table 1), yet the droplet volume rate is larger by an order of magnitude (Fig. 6b). Also, a shift to larger sizes at high VFR can be seen in the observed droplet size distributions (Fig. 3c, d). One possible explanation for a shift of the droplet size distribution to larger sizes might be coalescence of droplets, leading to a larger fraction of large droplets that cannot efficiently transfer particles from water to air. Another potential explanation for the more efficient water–air transfer of microplastic particles could be the more efficient scavenging of suspended microplastic particles by rising bubbles at low VFR.

Interestingly, for particle diameters up to 1.0 µm, transfer factors larger than 1 were observed. This means that the MP particle concentration in the droplet was enhanced compared to the bulk water concentration. These findings are consistent with earlier studies by Blanchard and Syzdek [9] and Bezdek and Carlucci [7], who found enhanced bacterial concentrations in jet drops due to enrichment of suspended bacteria at the water–gas interface of rising bubbles. Similarly, enrichment of suspended MP particles at the interface of rising bubbles was expected in the present experiment. It must be noted that the observed enrichment is likely an underestimation due to additional loss processes of airborne droplets and MP particles. For example, a fraction of 4.3% to 5.1% of the jet drops ejected by bubble bursting reached a height of 10 cm or more in the experiments at VFR = 182 mm^3 s^{-1} to VFR = 353 mm^3 s^{-1}, and thus, were lost to the glass flask wall. Clearly, the transfer factors shown in Fig. 6a increase with increasing particle diameter from 0.35 µm to 1 µm. This observation was made for both VFRs, and it suggests a size-dependent transfer

efficiency of MP particles by bubble bursting. Under the experimental conditions of this study, MP particles with a diameter of 1.0 µm were transferred most efficiently from water to air by bubble bursting. The decrease of the transfer factor for particle diameters greater than 1 µm may be an artifact due to the low particle number concentrations and the large uncertainties in the 1.5 µm and 2 µm diameter experiments. The presented findings indicate that particle enrichment at the interface of the rising bubble, bubble size distributions and the resulting droplet size distributions, as well as droplet and particle loss processes in the glass flask contribute to changes of the observed airborne MP particle concentrations. Particle enrichment and particle loss processes are expected to be dependent on particle size, and it is not possible to fully disentangle these size-dependencies within this study. It must be noted that the burst rate per unit area of water surface is in the upper range of the average estimate of natural bubble bursting in the oceans, and bubble diameters observed in our experiments tend to be larger than the majority of bubbles in sea water. Also, the transfer efficiency in natural waters, as mentioned before, is certainly affected by additional factors such as water salinity or surface tension, and the presented results should not be applied directly to natural systems. Nevertheless, we conclude that particle size must be taken into account in future parameterizations of the water–air transfer of MP particles.

Recently, Masry et al. [27] demonstrated in their lab experiments that bubble bursting can transfer MP particles from water to air. Their experimental setup was similar to ours in principle, however, with larger water and air volumes, uncharacterized bubble and droplet size spectra but probably a much larger droplet volume compared to this study. In their study, they clearly demonstrate the water–air transfer of 0.35 µm polystyrene particles but do not distinguish 0.6 and 1.0 µm particles from background concentrations. Given the fact that the water–air transfer factor was highest for 1.0 µm polystyrene particles in the present study, it can be speculated that the water concentration of the larger particles was too low, similar to the experiments using 1.5 and 2.0 µm particles in this study. Also, it must be noted that the observed decrease in transfer factors with increasing volume flow rates for droplet generation suggests less effective water–air transfer of particles in their experiments in general.

Environmental implications

Even though the presented size-dependent water–air transfer factors of MP particles are associated with large uncertainties, this study corroborates the hypothesis that oceans (and other water bodies) can act as sources of airborne MP particles. Recently, Lehmann et al. [25] investigated the ejection of marine MP particles by impacting rain droplets, and estimated an upper boundary on the order of 10^{14} MP particles ejected per year globally. Due to the large uncertainties associated with MP particle concentrations in marine waters, we do not attempt to extrapolate our findings to the global scale but rather compare the relative efficiency of the water–air-transfer processes due to impacting rain droplets and due to bubble bursting. To do this, we follow the assumptions made in Lehmann et al. [25] and only consider jet droplets with diameters less than 200 µm which are likely to be picked up by wind under the typical conditions at the ocean surface. The ocean surface water concentration of MP particles assumed in this calculation is 2.9 MP particles per liter according to Choy et al. [15]. It must be noted that MP concentrations in the oceans are expected to greatly vary in time and space, and MP particles with diameters < 2 µm used in this study are certainly underrepresented in measurements of sea surface MP concentrations due to limitations in sampling and analytical techniques. Since most film droplets are smaller than 1 µm in radius (e.g. [17]), it can be expected that supermicron MP particles are transferred from water to air mostly by jet droplets (e.g. [33]). In order to estimate ambient droplet volume fluxes of ocean sea spray, we use Eqs. S2.4 – S2.7 (supplementary material) to calculate a jet droplet size distribution at formation according to Andreas [5] and Monahan et al. [28]. With an average wind speed of 8 m s^{-1}, we calculate a total volume flux of droplets smaller than 200 µm diameter of 1.5×10^{-8} l m^{-2} s^{-1}. With the total surface area of the global oceans of approximately 3.61×10^{14} m^2, the total annual droplet volume flux is 1.7×10^{14} l.

Assuming the particle concentration in jet droplets is the same as in the bulk water at the ocean surface, this results in an estimated 5×10^{14} particles per year globally that are ejected in droplets small enough to potentially enter atmospheric uptake by wind. Taking into account the enrichment of MP particles in jet droplets, with an MP concentration in jet droplets enhanced by a factor ranging from 3 (as observed in this study) to 200 (as observed e.g. by [32]), the global emission estimate of MP particles from oceans by bubble bursting ranges from 10^{15} to 10^{17} particles per year. This is 10 to 1000 times larger than the estimated 10^{14} MP particles per year by impacting raindrops. There are various uncertainties affecting these estimates including (1) uncertainties of the size distribution of the jet droplets, (2) the rate of bursting bubbles on global oceans, and (3) MP concentrations in the ocean surface water. Nevertheless, this estimate indicates that bubble bursting is an effective water–air transfer process for MP particles in the environment.

Conclusions

The results of this study demonstrate that submicron MP particles are readily transferred from water to air by bubble bursting. This supports the hypothesis that oceans (and other water bodies) can act as sources of atmospheric MP particles. Compared with the ejection of MP particles by impacting rain droplets, bubble bursting is estimated to be more efficient by a factor of 10 to 1000. The experimentally determined water–air transfer factors are dependent on particle size and the droplet volume flow rate, with a maximum for 1 µm particles at low volume flow rate. For particle diameters up to 1.0 µm, MP particle concentrations are found to be larger in the droplet than in the bulk water. The enhanced concentration of MP particles in droplets compared to the bulk water concentration can be explained by enrichment of MP particles at the water–gas interface of rising bubbles, as previously discussed by Quinn et al. [31] and Sakai et al. [32]. Hence, bubble bursting may not only be a highly efficient transfer mechanism for MP particles from water to air but also, rising gas bubbles may be an important vertical transport process of MP particles in the water column, potentially contributing to the enrichment of MP particles in the sea surface microlayer. While the water–air transfer of MP particles with diameters larger than 1.0 µm could not be quantified, it should be noted that this is very likely due to experimental limitations such as low particle concentrations, relatively high background concentrations, a low sampling flow rate, and particle losses in the experimental setup. Therefore, the presented experiments do not allow conclusions regarding the water–air transfer of MP particles larger than 1.0 µm. In future work, it is also important to investigate the effects of surfactants and water salinity on the bubble bursting process and the water–air transfer of MP particles, which is expected to play a role in natural waters [27].

Supplementary Information

The online version contains supplementary material available at https://doi.org/10.1186/s43591-023-00079-x.

Additional file 1: Supplementary Material. Water-air transfer rates of microplastic particles through bubble bursting as a function of particle size. **Table S1.** Particle size, concentration of particles in suspension c_{susp}, supplied volume of suspension V_{susp} and number of particles in water N_w. **Figure S3.** Temporal evolution of the observed airborne particle concentration (black line) corresponding to (a) 0.35 µm and (b) 1.0 µm diameter MP particles, and the expected airborne MP concentration acc. Eqs. 1 and 2 (main manuscript, green line). Vertical dashed red lines indicate valve switching between two glass flasks. The two experiments were carried out in parallel.

Acknowledgements
The authors acknowledge fruitful discussions with collaborators in the SFB Mikroplastik consortium.

Authors' contributions
LMO was responsible for conceptualization, methodology, investigation and writing. SS contributed to methodology, investigation and writing. ML contributed to formal analysis and writing. SG contributed to project administration and funding acquisition. AH was responsible for project administration, funding acquisition, conceptualization, writing and resources. LMO, SS and AH contributed to visualization. SS, ML, SG and AH contributed to review and editing.

Funding
Open Access funding enabled and organized by Projekt DEAL. This work was funded by the Deutsche Forschungsgemeinschaft (DFG, German Research Foundation) – Project Number 391977956 – SFB1357.

Availability of data and materials
The datasets used and/or analysed during the current study are available from the corresponding author on reasonable request.

Declarations

Ethics approval and consent to participate
Not applicable.

Consent for publication
Not applicable.

Competing interests
The authors declare no competing interests.

Received: 5 December 2022 Accepted: 27 December 2023
Published online: 10 January 2024

References

1. Allen S, Allen D, Phoenix VR, Le Roux G, Durántez Jiménez P, Simonneau A, Binet S, Galop D. Atmospheric transport and deposition of microplastics in a remote mountain catchment. Nat Geosci. 2019;12:339–44. https://doi.org/10.1038/s41561-019-0335-5.
2. Allen S, Allen D, Moss K, Le Roux G, Phoenix VR, Sonke JE. Examination of the ocean as a source for atmospheric microplastics. Plos One. 2020;15(5):e0232746. https://doi.org/10.1371/journal.pone.0232746.
3. Aller JY, Kuznetsova MR, Jahns CJ, Kemp PF. The sea surface microlayer as a source of viral and bacterial enrichment in marine aerosols. J Aerosol Sci. 2005;36:801–12.
4. Anderson ZT, Cundy AB, Croudace IW, Warwick PE, Celis-Hernandez O, Stead JL. A rapid method for assessing the accumulation of microplastics in the sea surface microlayer (SML) of estuarine systems. Sci Rep. 2018;8:9428.
5. Andreas EL. Thermal and size evolution of sea spray droplets. Hanover: CRREL report 89–11, US Army Corps of Engineers Cold Regions Research & Engineering Laboratory; 1989.
6. Bettaieb A, Filali A, Filali T, Aissia HB. An efficient algorithm for overlapping bubbles segmentation. Comput Opt. 2020;44:363–74. https://doi.org/10.18287/2412-6179-CO-605.
7. Bezdek HF, Carlucci AF. Surface concentration of marine bacteria. Limnol Oceanogr. 1972;17:566–9.
8. Bigg EK, Leck C. The composition of fragments of bubbles bursting at the ocean surface. J Geophys Res. 2008;113:D11209.
9. Blanchard DC, Syzdek L. Mechanism for the water-to-air transfer and concentration of bacteria. Science. 1970;170:626–8.
10. Blanchard DC. The ejection of drops from the sea and their enrichment with bacteria and other materials: a review. Estuaries. 1989;12(3):127–37.
11. Brahney J, Hallerud M, Heim E, Hahnenberger M, Sukumaran S. Plastic rain in protected areas of the United States. Science. 2020;368(6496):1257–60.
12. Browne MA, Crump P, Niven SJ, Teuten E, Tonkin A, Galloway T, Thompson R. Accumulation of microplastic on shorelines woldwide: sources and sinks. Environ Sci Technol. 2011;45:9175–9. https://doi.org/10.1021/es201811s.

13. Chae D-H, Kim I-S, Kim S-K, Song YK, Shim WJ. Abundance and distribution characteristics of microplastics in surface seawaters of the Incheon/Kyeonggi coastal region. Arch Environ Contam Toxicol. 2015;69:269–78.
14. Chen G, Feng Q, Wang J. Mini-review of microplastics in the atmosphere and their risks to humans. Sci Total Environ. 2020;703:135504. https://doi.org/10.1016/j.scitotenv.2019.135504.
15. Choy CA, Robison BH, Gagne TO, Erwin B, Firl E, Halden RU, Hamilton JA, Katija K, Lisin SE, Rolsky C, Van Houtan KS. The vertical distribution and biological transport of marine microplastics across the epipelagic and mesopelagic water column. Sci Rep. 2019;9:7843. https://doi.org/10.1038/s41598-019-44117-2.
16. Cormier B, Gambardella C, Tato T, Perdriat Q, Costa E, Veclin C, Le Bihanic F, Grassl B, Dubocq F, Kärrman A, Van Arkel K, Lemoine S, Lagarde F, Morin B, Garaventa F, Faimali M, Cousin X, Bégout M-L, Beiras R, Cachot J. Chemicals sorbed to environmental microplastics are toxic to early life stages of aquatic organisms. Ecotoxicol Environ Saf. 2021;208:111665. https://doi.org/10.1016/j.ecoenv.2020.111665.
17. de Leeuw G, Andreas EL, Anguelova, MD, Fairall CW, Lewis ER, O'Dowd C, Schulz E, Schwartz SE, 2011. Production flux of sea spray aerosol. Rev Geophys 49 (2001). https://doi.org/10.1029/2010RG000349.
18. Engel A, Bange HW, Cunliffe M, Burrows SM, Friedrichs G, Galgani L, Herrmann H, Hertkorn N, Johnson M, Liss PS, Quinn PK, Schartau M, Soloviev A, Stolle C, Upstill-Goddard RC, van Pinxteren M, Zäncker B. The ocean's vital skin: toward an integrated understanding of the sea surface microlayer. Front Mar Sci. 2017;4:165.
19. Enyoh CE, Verla AW, Verla EN, Ibe FC, Amaobi CE. Airborne microplastics: a review study on method for analysis, occurrence, movement and risks. Environ Monit Assess. 2019;191:290–3. https://doi.org/10.1016/j.marpolbul.2016.01.006.
20. Gallo F, Fossi C, Weber R, Santillo D, Sousa J, Ingram I, Nadal A, Romano D. Marine litter plastics and microplastics and their toxic chemicals components: the need for urgent preventive measures. Environ Sci Eur. 2018;30:13. https://doi.org/10.1186/s12302-018-0139-z.
21. Gañán-Calvo AM. Revision of bubble bursting: Universal scaling laws of top jet drop size and speed. Phys Rev Lett. 2017;119:204502.
22. Ghabache E, Séon T. Size of the top jet drop produced by bubble bursting. Phys Rev Fluids. 2016;1:051901. https://doi.org/10.1103/PhysRevFluids.1.051901.
23. Huang Y, Qing X, Wang W, Han G, Wang J. Mini-review on current studies of airborne microplastics: analytical methods, occurrence, sources, fate and potential risk to human beings. TrAC Trends Analyt Chem. 2020;125:115821.
24. Kočárková H, Rouyer F, Pigeonneau F, 2013. Film drainage of viscous liquid on top of bare bubble: Influence of the Bond number. Phys Fluids 25. https://doi.org/10.1063/1.4792310.
25. Lehmann M, Oehlschlägel LM, Häusl FP, Held A, Gekle S. Ejection of marine microplastics by raindrops: a computational and experimental study. Microplast Nanoplast. 2021;1:18. https://doi.org/10.1186/s43591-021-00018-8.
26. Liu K, Wu T, Wang X, Song Z, Zong C, Wei N, Li D. Consistent transport of terrestrial microplastics to the ocean through atmosphere. Environ Sci Technol. 2019;53:10612–9. https://doi.org/10.1021/acs.est.9b03427.
27. Masry M, Rossignol S, TemimeRoussel B, Bourgogne D, BussièreR'mili P-OB, Wong-Wah-Chung P. Experimental evidence of plastic particles transfer at the water-air interface through bubble bursting. Environ Pollut. 2021;280:116949. https://doi.org/10.1016/j.envpol.2021.116949.
28. Monahan, E.C., Spiel D.E., Davidson, K.L., 1986. A model of marine aerosol generation via whitecaps and wave disruption. Monahan, E.C., Mac Niocaill, G. (Eds.) Oceanic whitecaps and their role in air–sea exchange processes. Springer, Dordrecht, 167–174. https://doi.org/10.1007/978-94-009-4668-2
29. Polysciences (2022) https://www.polysciences.com/german/polybead-microspheres-035956m. Last access on 20 June 2022
30. Prata JC. Airborne microplastics: consequences to human health? Environ Pollut. 2018;234:115e126. https://doi.org/10.1016/j.envpol.2017.11.043.
31. Quinn JA, Steinbrook RA, Anderson JL. Breaking bubbles and the water-to-air transport of particulate matter. Chem Eng Sci. 1975;30:1177–84.
32. Sakai M, Tanaka A, Egawa H, Sugihara G. Enrichment of suspended particles in top jet drops from bursting bubbles. J Coll Interface Sci. 1988;125:428–36.
33. Shaw DB, Li Q, Nunes JK, Deike L. Ocean emission of microplastic. PNAS Nexus. 2023;2:1–11. https://doi.org/10.1093/pnasnexus/pgad296.
34. Song YK, Hong SH, Jang M, Kang J-H, Kwon OY, Han GM, Shim WJ. Large accumulation of micro-sized synthetic polymer particles in the sea surface microlayer. Environ Sci Technol. 2014;48:9014–21.
35. Spiel DE. On the births of jet drops from bubbles bursting on water surfaces. J Geophys Res. 1995;100:4995–5006. https://doi.org/10.1029/94JC03055.
36. Spiel DE. A hypothesis concerning the peak in film drop production as a function of bubble size. J Geophys Res. 1997;102:1153–61.
37. Spiel DE. On the births of film drops from bubbles bursting on seawater surfaces. J Geophys Res. 1998;103:24907–18.
38. Trainic M, Flores JM, Pinkas I, Pedrotti ML, Lombard F, Bourdin G, Gorsky G, Boss E, Rudich Y, Vardi A, Koren I. Airborne microplastic particles detected in the remote marine atmosphere. Commun Earth Environ. 2020;1:64. https://doi.org/10.1038/s43247-020-00061-y.
39. Wang X, Deane GB, Moore KA, Ryder OS, Stokes MD, Beall CM, Collins DB, Santander MV, Burrows SM, Sultana CM, Prather KA. The role of jet and film drops in controlling the mixing state of submicron sea spray aerosol particles. Proc Natl Acad Sci. 2017;114:6978–83.
40. Wurl O, Wurl E, Miller L, Johnson K, Vagle S. Formation and global distribution of sea-surface microlayers. Biogeosciences. 2011;8:121–35.
41. Zhang K, Su J, Xiong X, Wu X, Wu C, Liu J. Microplastic pollution of lakeshore sediments from remote lakes in Tibet plateau. China Environ Pollut. 2016;219:450–5. https://doi.org/10.1016/j.envpol.2016.05.048.
42. Zhang Y, Kang S, Allen S, Allen D, Gao T, Sillanpää M. Atmospheric microplastics: a review on current status and perspectives. Earth Sci Rev. 2020;203:103118. https://doi.org/10.1016/j.earscirev.2020.103118.

Publisher's Note